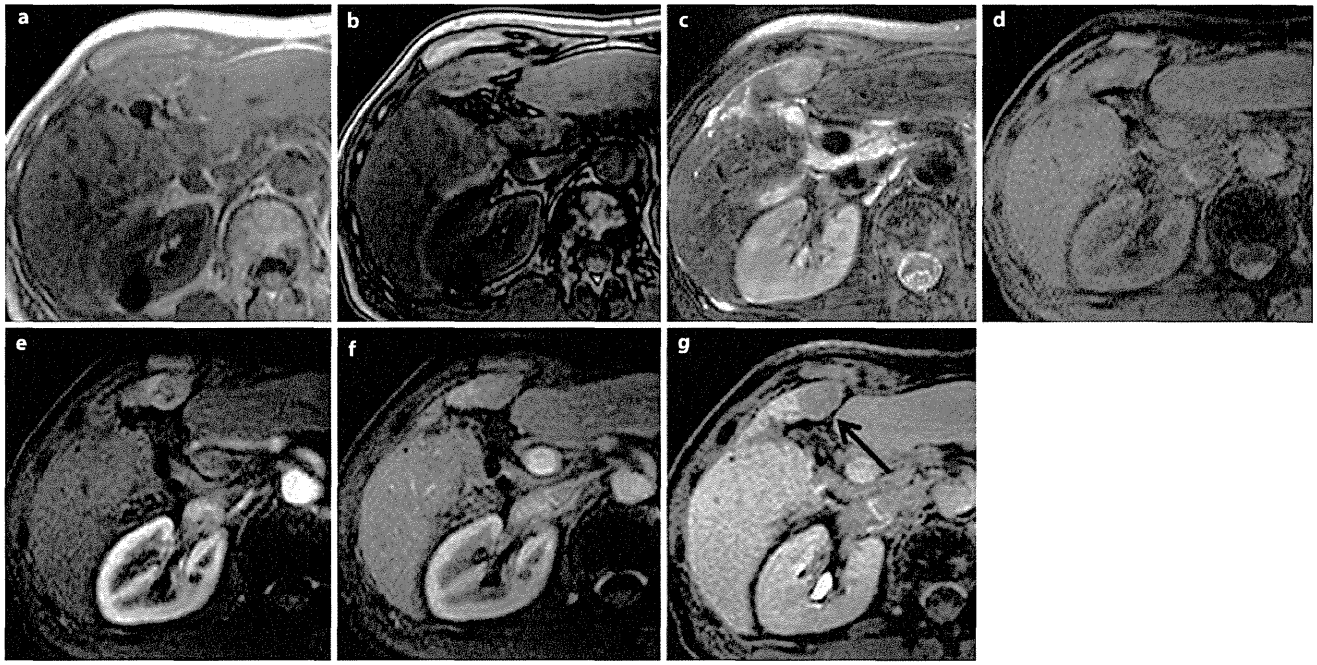

Fig. 12. Gd-EOB-DTPA-enhanced MRI of hypervascular HCC in chronic hepatitis C: T_1-weighted (in-phase) image (**a**), T_1-weighted (opposed phase) (**b**), T_2-weighted (**c**), precontrast 3DFT T_1-weighted image (**d**), arterial phase (**e**), PVP (**f**), and hepatocyte phase (**g**). In-phase T_1-weighted (**a**) and opposed phase T_1-weighted images (**b**) reveal no fat deposition in the tumor. The tumor shows high intensity on the T_2-weighted image (**c**). The tumor shows hypointensity relative to the liver parenchyma on the precontrast 3DFT T_1-weighted image (**d**), but marked enhancement of HCC can be seen in the arterial phase (**e**). The tumor shows hypointensity in the PVP (**f**), and hypointensity in the hepatocyte phase which is the most important phase for detection of the tumor (**g**; arrow).

MRI with T_1-weighted fast imaging sequence. Functioning hepatocytes take up Gd-EOB-DTPA in the hepatocyte phase, which occurs approximately 15–20 min after injection. Gd-EOB-DTPA works as a T_1-shortening agent at the hepatocyte phase after injection. Thus, malignant liver lesions such as HCC and liver metastases are spared the contrast uptake that occurs in the surrounding liver parenchyma. Both Gd-EOB-DTPA and SPIO have been designed to overcome the limitations of nonspecific tissue uptake of extracellular low-molecular Gd-DTPA [50, 51] (fig. 12).

As Gd-EOB-DTPA-enhanced MRI employs 3DFT fast imaging sequence with high spatial resolution, it can detect more tiny nodules relative to SPIO-enhanced MRI. In particular, as the spatial resolution of the longitudinal axis of the body has improved on the MR sequence, it is easy to differentiate a tiny nodule from vessels with thin slice images. It was reported that Gd-EOB-DTPA-enhanced MRI is superior in the detection of HCC to dynamic MDCT and dynamic MRI with Gd-DTPA [52, 53]. It is particularly hard to detect small hypovascular HCC on dynamic MDCT and dynamic MRI with Gd-DTPA, because it does not show arterial enhancement and only shows a mild washout of contrast medium in the portal venous and equilibrium phases. Moreover, as hypovascular HCC is usually well-differentiated HCC with Kupffer cells, it uptakes SPIO and shows hypo- or isointensity relative to the liver parenchyma on SPIO-enhanced MRI, resulting in low detection sensitivity. However, Gd-EOB-DTPA-enhanced MRI can show HCC as hypointensity relative to the liver parenchyma, not depending on histological differentiation of the HCC [9, 10]. After all, Gd-EOB-DTPA-enhanced MRI shows higher detection sensitivity for not only hypervascular HCC but also hypovascular HCC than dynamic MDCT and dynamic MRI with Gd-DTPA. Compared with SPIO-enhanced MRI, Gd-EOB-DTPA-enhanced MRI also shows higher detection sensitivity for hypovascular HCC and the same detection sensitivity for hypervascular HCC [10].

Fig. 13. Gd-EOB-DTPA-enhanced MRI of hypervascular HCC in chronic hepatitis B: T_2-weighted image (**a**), precontrast 3DFT T_1-weighted image (**b**), arterial phase (**c**), PVP (**d**), hepatocyte phase (**e**), CTAP (**f**), and CTHA (**g**). **e** Hepatocyte phase image of Gd-EOB-DTPA-enhanced MRI can detect HCC the same as CTAP and CTHA.

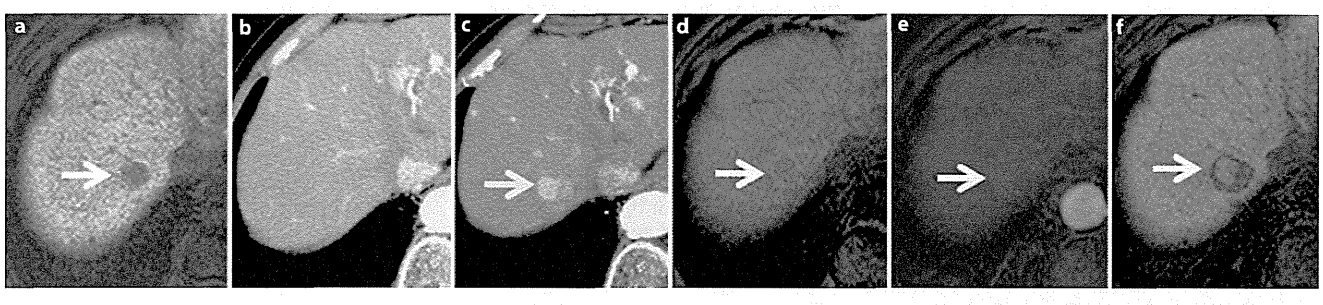

Fig. 14. Chronic hepatitis C. Hypovascular nodule (arrows in **a** and **c–f**) found on hepatobiliary phase of Gd-EOB-DTPA-enhanced MRI, followed by arterial hypervascularization 1 year later. **a** Axial contrast-enhanced hepatobiliary phase MR image shows a hepatic nodule in liver segment 7. The nodule had neither arterial enhancement nor washout in the dynamic MR study (not shown). **b** Arterial phase of dynamic CT taken 2 months after initial MRI shows no corresponding arterial enhancement. **c** A follow-up CT 1 year after initial MRI shows arterial enhancement of the nodule. **d–f** MRI was performed the next day. **d** Precontrast 3DFT T_1-weighted MR image shows decreased signal intensity in the nodules. **e** Arterial phase of contrast after Gd-EOB-DTPA injection shows slight enhancement of the nodule. **f** Hepatobiliary phase image reveals the nodule with focal defect in contrast and nodule-in-nodule pattern (hyperintense foci in hypointense nodule). The diameter of the nodule increased from 14 to 21 mm (tumor volume doubling time, 216 days). US-guided fine-needle biopsy (not shown) revealed well-differentiated HCC.

Role of CTAP and CTHA

Recently, the number of instances where only CTAP and CTHA are performed for the diagnosis of HCC is decreasing. CTAP and CTHA are usually only performed for the final decision of the treatment area at the time of transcatheter arterial chemoembolization. However, CTAP and CTHA are still believed to be a most reliable imaging method to decide on the treatment strategy because the nodule with partial portal perfusion defect or increasing arterial flow has a high possibility to be a typical hypervascular HCC [54]. Gd-EOB-DTPA-enhanced MRI has the same detection sensitivity of both hyper- and hypovascular HCC such as CTAP and CTHA [10] (fig. 13). After all, Gd-EOB-DTPA-enhanced MRI is the best noninvasive imaging method for the detection of HCC, and may replace invasive imaging methods of CTAP and CTHA.

Management of Tiny Hypovascular Nodule Detected Only on Gd-EOB-DTPA-Enhanced MRI

Recently, Gd-EOB-DTPA-enhanced MRI is frequently performed when screening high-risk patients for HCC, and we often encounter tiny hypovascular nodules of less than 15 mm in diameter; these can only be detected as hypointensity nodules on the hepatocyte phase images of Gd-EOB-DTPA-enhanced MRI (fig. 14). Clinical management of these tiny hypovascular nodules is now discussed. It is neither clinically realistic nor cost-effective to employ invasive examination methods such as CTAP and CTHA for these tiny hypovascular nodules. The hypovascular tiny nodules with a doubling time of less than 300 days show hypervascularization of the tumor at a high rate during follow-up [unpublished data] (fig. 14). So, the follow-up study with Gd-EOB-DTPA-enhanced MRI including evaluation of doubling time of these tiny hypovascular nodules is useful and can avoid using invasive examination methods such as CTAP and CTHA.

Disclosure Statement

None of the authors have any conflicts of interest associated with this paper.

References

1 Kim TK, Lee KH, Khalili K, Jang HJ: Hepatocellular nodules in liver cirrhosis: contrast-enhanced ultrasound. Abdom Imaging 2011;36:244–263.
2 Murakami T, Onishi H, Mikami K, et al: Determining the optimal timing for early arterial phase hepatic CT imaging by measuring abdominal aortic enhancement in variable contrast injection protocols. J Comput Assist Tomogr 2006;30:206–211.
3 Takahashi S, Murakami T, Takamura M, et al: Multi-detector row helical CT angiography of hepatic vessels: depiction with dual-arterial phase acquisition during single breath hold. Radiology 2002;222:81–88.
4 Hashimoto K, Murakami T, Dono K, et al: Quantitative tissue blood flow measurement of the liver parenchyma: comparison between xenon CT and perfusion CT. Dig Dis Sci 2007;52:943–949.
5 Noguchi Y, Murakami T, Kim T, Hori M, Osuga K, Kawata S, Kumano S, Okada A, Sugiura T, Nakamura H: Detection of hepatocellular carcinoma: comparison of dynamic MR imaging with dynamic double arterial phase helical CT. AJR Am J Roentgenol 2003; 180:455–460.
6 Imai Y, Murakami T, Yoshida S, et al: Superparamagnetic iron oxide-enhanced MR images of hepatocellular carcinoma: correlation with histological grading. Hepatology 2000;32:205–212.
7 Saito K, Kotake F, Ito N, et al: Gd-EOB-DTPA enhanced MRI for hepatocellular carcinoma: quantitative evaluation of tumor enhancement in hepatobiliary phase. Magn Reson Med Sci 2005;4:1–9.
8 Tsuda N, Okada M, Murakami T: Potential of gadolinium-ethoxybenzyl-diethylenetriamine pentaacetic acid (Gd-EOB-DTPA) for differential diagnosis of nonalcoholic steatohepatitis and fatty liver in rats using magnetic resonance imaging. Invest Radiol 2007; 42:242–247.
9 Kogita S, Imai Y, Okada M, Kim T, Onishi H, Takamura M, Fukuda K, Igura T, Sawai Y, Morimoto O, Hori M, Nagano H, Wakasa K, Hayashi N, Murakami T: Gd-EOB-DTPA-enhanced magnetic resonance images of hepatocellular carcinoma: correlation with histological grading and portal blood flow. Eur Radiol 2010;20:2405–2413.
10 Okada M, Imai Y, Kim T, Kogita S, Takamura M, Kumano S, Onishi H, Hori M, Fukuda K, Hayashi N, Wakasa K, Sakamoto M, Murakami T: Comparison of enhancement patterns of histologically confirmed hepatocellular carcinoma between gadoxetate- and ferucarbotran-enhanced magnetic resonance imaging. J Magn Reson Imaging 2010;32:903–913.
11 Kagawa Y, Okada M, Kumano S, Katsube T, Imaoka I, Tanigawa N, Kudo M, Ishii K, Murakami T: Optimal scanning protocol of arterial dominant phase for hypervascular hepatocellular carcinoma with gadolinium-ethoxybenzyl-diethylenetriamine pentaacetic acid-enhanced MR. J Magn Reson Imaging 2011;33:864–872.
12 Bruix J, Sherman M: Management of hepatocellular carcinoma: an update. Hepatology 2011;53:1020–1022.
13 Burns PN, Wilson SR: Microbubble contrast for radiological imaging. 1. Principles. Ultrasound Q 2006;22:5–13.
14 Brannigan M, Burns PN, Wilson SR: Blood flow patterns in focal liver lesions at microbubble-enhanced US. Radiographics 2004; 24:921–935.
15 Matsui O, Kadoya M, Kameyama T, et al: Benign and malignant nodules in cirrhotic livers: distinction based on blood supply. Radiology 1991;178:493–497.
16 Hayashi M, Matsui O, Ueda K, et al: Correlation between the blood supply and grade of malignancy of hepatocellular nodules associated with liver cirrhosis: evaluation by CT during intraarterial injection of contrast medium. AJR 1999;172:969–976.
17 Jang HJ, Kim TK, Burns PN, Wilson SR: Enhancement patterns of hepatocellular carcinoma at contrast-enhanced US: comparison with histologic differentiation. Radiology 2007;244:898–906.
18 Bhayana D, Kim TK, Jang HJ, Burns PN, Wilson SR: Hypervascular liver masses on contrast-enhanced ultrasound: the importance of washout. AJR 2010;194:977–983.
19 Moriyasu F, Itoh K: Efficacy of perflubutane microbubble-enhanced ultrasound in the characterization and detection of focal liver lesions: phase 3 multicenter clinical trial. AJR Am J Roentgenol 2009;193:86–95.
20 Luo W, Numata K, Morimoto M, et al: Focal liver tumors: characterization with 3D perflubutane microbubble contrast agent-enhanced US versus 3D contrast-enhanced multidetector CT. Radiology 2009;251:287–295.
21 Kudo M, Hatanaka K, Kumada T, et al: Double-contrast ultrasound: a novel surveillance tool for hepatocellular carcinoma. Am J Gastroenterol 2011;106:368–370.
22 Luo W, Numata K, Morimoto M, et al: Role of Sonazoid-enhanced three-dimensional ultrasonography in the evaluation of percutaneous radiofrequency ablation of hepatocellular carcinoma. Eur J Radiol 2010;75:91–97.
23 Yanagisawa K, Moriyasu F, Miyahara T, Yuki M, Iijima H: Phagocytosis of ultrasound contrast agent microbubbles by Kupffer cells. Ultrasound Med Biol 2007;33:318–325.
24 Minami Y, Chung H, Kudo M, et al: Radiofrequency ablation of hepatocellular carcinoma: value of virtual CT sonography with magnetic navigation. AJR Am J Roentgenol 2008;190:W335–W341.

25 Cuenod C, Leconte I, Siauve N, et al: Early changes in liver perfusion caused by occult metastases in rats: detection with quantitative CT. Radiology 2001;218:556–561.
26 Cenic A, Nabavi DG, Craen RA, Gelb AW, Lee TY: Dynamic CT measurement of cerebral blood flow: a validation study. AJNR Am J Neuroradiol 1999;20:63–73.
27 Willett CG, Boucher Y, di Tomaso E, et al: Direct evidence that the VEGF-specific antibody bevacizumab has antivascular effects in human rectal cancer. Nat Med 2004;10: 145–147.
28 Ma SH, Le HB, Jia BH, et al: Peripheral pulmonary nodules: relationship between multi-slice spiral CT perfusion imaging and tumor angiogenesis and VEGF expression. BMC Cancer 2008;8:186.
29 Ippolito D, Sironi S, Pozzi M, et al: Hepatocellular carcinoma in cirrhotic liver disease: functional computed tomography with perfusion imaging in the assessment of tumor vascularization. Acad Radiol 2008;15:919–927.
30 Llovet JM, Ricci S, Mazzaferro V, et al: Sorafenib in advanced hepatocellular carcinoma. N Engl J Med 2008;359:378–390.
31 Okada M, Kim T, Murakami T: Hepatocellular nodules in liver cirrhosis: state of the art CT evaluation (perfusion CT/volume helical shuttle scan/dual-energy CT, etc.). Abdom Imaging 2011;36:273–281.
32 Bader TR, Herneth AM, Blaicher W, et al: Hepatic perfusion after liver transplantation: noninvasive measurement with dynamic single-section CT. Radiology 1998; 209:129–134.
33 Hashimoto K, Murakami T, Dono K, et al: Assessment of the severity of liver disease and fibrotic change: the usefulness of hepatic CT perfusion imaging. Oncol Rep 2006;16: 677–683.
34 Genant HK, Boyd D: Quantitative bone mineral analysis using dual energy computed tomography. Invest Radiol 1977;12:545–551.
35 Brooks RA: A quantitative theory of the Hounsfield unit and its application to dual energy scanning. J Comput Assist Tomogr 1977;1:487–493.
36 Nakayama Y, Awai K, Funama Y, et al: Abdominal CT with low tube voltage: preliminary observations about radiation dose, contrast enhancement, image quality, and noise. Radiology 2005;237:945–951.
37 Yeh BM, Shepherd JA, Wang ZJ, et al: Dual-energy and low-kVp CT in the abdomen. AJR Am J Roentgenol 2009;193:47–54.
38 Schindera ST, Nelson RC, Mukundan S Jr, et al: Hypervascular liver tumors: low tube voltage, high tube current multi-detector row CT for enhanced detection – phantom study. Radiology 2008;246:125–132.
39 Marin D, Nelson RC, Samei E, et al: Hypervascular liver tumors: low tube voltage, high tube current multidetector CT during later hepatic arterial phase for detection – initial clinical experience. Radiology 2009;251: 771–779.
40 Reimer P, Rummeny EJ, Daldrup HE, et al: Clinical results with Resovist: a phase 2 clinical trial. Radiology 1995;195:489–496.
41 Saini S, Stark DD, Hahn PF, et al: Ferrite particles: a superparamagnetic MR contrast agent for enhanced detection of liver carcinoma. Radiology 1987;162:217–222.
42 Ferrucci JT, Stark DD: Iron oxide-enhanced MR imaging of the liver and spleen: review of the first 5 years. AJR Am J Roentgenol 1990;155:943–950.
43 Yamamoto H, Yamashita Y, Yoshimatsu S, et al: Hepatocellular carcinoma in cirrhotic livers: detection with unenhanced and iron oxide-enhanced MR imaging. Radiology 1995; 195:106–112.
44 Hori M, Murakami T, Kim T, et al: Detection of hypervascular hepatocellular carcinoma: comparison of SPIO-enhanced MRI with dynamic helical CT. J Comput Assist Tomogr 2002;26:701–710.
45 Kim YK, Kwak HS, Kim CS, Chung GH, Han YM, Lee JM: Hepatocellular carcinoma in patients with chronic liver disease: comparison of SPIO-enhanced MR imaging and 16-detector row CT. Radiology 2006;238: 531–541.
46 Imai Y, Murakami T, Hori M, et al: Hypervascular hepatocellular carcinoma: Combined dynamic MDCT and SPIO-enhanced MRI versus combined CTHA and CTAP. Hepatol Res 2008;38:147–158.
47 Yukisawa S, Okugawa H, Masuya Y, et al: Multidetector helical CT plus superparamagnetic iron oxide-enhanced MR imaging for focal hepatic lesions in cirrhotic liver: a comparison with multi-phase CT during hepatic arteriography. Eur J Radiol 2007;61: 279–289.
48 Kim YK, Kwak HS, Han YM, et al: Usefulness of combining sequentially acquired gadobenate dimeglumine-enhanced magnetic resonance imaging and resovist-enhanced magnetic resonance imaging for the detection of hepatocellular carcinoma: comparison with computed tomography hepatic arteriography and computed tomography arterioportography using 16-slice multidetector computed tomography. J Comput Assist Tomogr 2007;31:702–711.
49 Hamm B, Staks T, Muhler A, et al: Phase I clinical evaluation of Gd-EOB-DTPA as a hepatobiliary MR contrast agent: safety, pharmacokinetics, and MR imaging. Radiology 1995;195:785–792.
50 Bellin MF, Vasile M, Morel-Precetti S: Currently used non-specific extracellular MR contrast media. Eur Radiol 2003;13:2688–2698.
51 Brasch RC: New directions in the development of MR imaging contrast media. Radiology 1992;183:1–11.
52 Di Martino M, Marin D, Guerrisi A, Baski M, Galati F, Rossi M, Brozzetti S, Masciangelo R, Passariello R, Catalano C: Radiology 2010;256:806–816.
53 Park G, Kim YK, Kim CS, Yu HC, Hwang SB: Diagnostic efficacy of gadoxetic acid-enhanced MRI in the detection of hepatocellular carcinomas: comparison with gadopentetate dimeglumine. Br J Radiol 2010;83: 1010–1016.
54 Hayashi M, Matsui O, Ueda K, et al: Progression to hypervascular hepatocellular carcinoma: correlation with intranodular blood supply evaluated with CT during intraarterial injection of contrast material. Radiology 2002;225:143–149.

J Gastroenterol (2011) 46:1238–1248
DOI 10.1007/s00535-011-0437-3

ORIGINAL ARTICLE—LIVER, PANCREAS, AND BILIARY TRACT

Evaluation of liver fibrosis by transient elastography using acoustic radiation force impulse: comparison with Fibroscan®

Hirotoshi Ebinuma · Hidetsugu Saito · Mina Komuta · Keisuke Ojiro · Kanji Wakabayashi · Shingo Usui · Po-sung Chu · Rumiko Umeda · Yuka Ishibashi · Tetsurou Takayama · Masahiro Kikuchi · Nobuhiro Nakamoto · Yoshiyuki Yamagishi · Takanori Kanai · Kiyoshi Ohkuma · Michiie Sakamoto · Toshifumi Hibi

Received: 22 December 2010 / Accepted: 8 June 2011 / Published online: 21 July 2011

Abstract
Background Accurate evaluation of liver fibrosis in patients with chronic liver damage is required to determine the appropriate treatment. Various approaches, including laboratory tests and transient elastography, have been used to evaluate liver fibrosis. Recently, transient elastography with acoustic radiation force impulse (ARFI) has been developed and applied with conventional ultrasonography. The aim of this study was to evaluate the clinical utility of transient elastography with ARFI and to compare the results with this method and those of the Fibroscan® procedure.
Methods One hundred and thirty-one patients with liver damage, who underwent liver biopsy at our department, were enrolled prospectively in this study. Elastography with ARFI (applied with ACUSON S2000®), and Fibroscan® was performed at the same time as liver biopsy. These measurements were compared with histological findings in liver biopsy specimens, and measurement accuracy was evaluated by receiver-operating characteristic analysis.
Results Elastography values with both procedures were significantly correlated with the stages of liver fibrosis and there was little difference in the results obtained using the 2 procedures. The accuracy of differential diagnosis between no fibrosis at F0 and more than F1 stage was insufficient with ARFI, but this procedure was sufficient for diagnosing advanced fibrosis. The accuracy of ARFI was almost equivalent to that of the Fibroscan® method. Moreover, both ARFI and Fibroscan® values increased in proportion to the severity of hepatic inflammation when fibrosis stage is low, but not in proportion to the severity of steatosis.
Conclusions Transient elastography with ARFI is simple, non-invasive and useful for diagnosing the stage of fibrosis in chronic liver disease. The utility of ARFI was almost equivalent to that of the Fibroscan® method.

Keywords Transient elastography · Acoustic radiation force impulse · Liver stiffness · Non-invasive · Fibrosis

Abbreviations

ARFI	Acoustic radiation force impulse
HCC	Hepatocellular carcinoma
US	Ultrasonography
ROI	Region of interest
ROC	Receiver operating characteristic
AUROC	Area under ROC curve

Introduction

The development of fibrotic changes in the liver is associated with the progression of chronic liver diseases and is

H. Ebinuma · H. Saito · K. Ojiro · K. Wakabayashi · S. Usui · P. Chu · R. Umeda · Y. Ishibashi · T. Takayama · M. Kikuchi · N. Nakamoto · Y. Yamagishi · T. Kanai · T. Hibi
Division of Gastroenterology and Hepatology, Department of Internal Medicine, School of Medicine, Keio University, Tokyo, Japan

H. Saito (✉)
Department of Internal Medicine, School of Medicine and Faculty of Pharmacy, Keio University, 35 Shinanomachi, Shinjuku-ku, Tokyo 160-8582, Japan
e-mail: hsaito@sc.itc.keio.ac.jp

M. Komuta · M. Sakamoto
Department of Pathology, School of Medicine, Keio University, Tokyo, Japan

K. Ohkuma
Department of Diagnostic Radiology, School of Medicine, Keio University, Tokyo, Japan

the result of hepatic wound healing following the continuous destruction of hepatocytes. In recent work, hepatic fibrosis has been viewed not as a static lesion, but as a lesion that may improve or worsen, dependent on the activity of these diseases [1]. The stage of fibrosis in chronic viral hepatitis correlates with the risk of hepatocarcinogenesis and decompensated cirrhosis, and successful anti-viral therapy results in decreases in the fibrosis stage and in the risk of the development of hepatocellular carcinoma (HCC).

Although needle biopsy is the gold standard for the evaluation of liver fibrosis in living patients [2], the procedure may be subject to sampling error, because only 1/50,000 of the entire liver is evaluated [3, 4], and the procedure may lead to complications including death [5]. Histological diagnosis is a subjective procedure and inter-observer and intra-observer differences in diagnoses sometimes occur [3]. Moreover, liver fibrosis occurs continuously, not stepwise, and fibrosis progresses finally to F4 stage. Laparoscopy is a macroscopic approach to the evaluation of liver fibrosis, but a recent report documented several cases in which the laparoscopic aspects and histological findings were disparate [6]. These findings suggest that an objective evaluation of liver fibrosis is required.

Transient elastography has been applied in the field of hepatology. The clinical usefulness of the Fibroscan® (EchoSens, Paris, France) device has been widely replicated following the first report of the technique by Sandrin et al. [7]. The Fibroscan® module uses a system in which external mechanical excitation is channeled into the liver and shear wave speeds are measured using ultrasonography (US). The elasticity of the liver is reduced by the accumulation of fibrosis, so that the measurement of elasticity correlates to the degree of liver fibrosis. We first reported the usefulness of Fibroscan® for measuring liver stiffness in Japanese patients with chronic hepatitis C [8]. In contrast, the technology of acoustic radiation force impulse (ARFI) is based on the principle of the mechanical excitation of tissue by short-duration acoustic pulses. This technology was initially used for imaging different materials in soft tissues clearly by producing shear waves with ARFI. Fahey et al. [9] first reported the efficacy of ARFI for detecting and monitoring the progression of human HCC and renal cancers. In 2008, Palmeri et al. [10] first described transient elastography of the human liver tissue using ARFI technology. Recently ARFI-assisted transient elastography was made commercially available in a US apparatus; this advance made it possible to measure the stiffness in a region of interest (ROI) chosen by the operator [11].

The aim of this study was to evaluate the clinical utility of transient elastography measured using ARFI technology and to compare these results and those obtained using the Fibroscan® method with the gold standard for the measurement of liver fibrosis in Japanese patients with various forms of liver injury.

Patients and methods

Enrolled patients

One hundred and thirty-one patients with liver damage, who underwent percutaneous liver needle biopsy at our department from October 2008 to October 2009, were enrolled prospectively in this study after receiving documentation of the purpose and methods and providing consent to participate.

Measurement of liver stiffness

Liver stiffness was measured by ARFI, using an ACUSON S2000® (Mochida Siemens Medical Systems, Tokyo, Japan), which enabled convenient and simple measurement of liver elasticity during US; and by Fibroscan® (EchoSens). Both procedures were performed at the same time as the percutaneous liver needle biopsy procedure, and the operators were blinded to the histology results. Measurement of liver stiffness using the ACUSON S2000® was performed by simply pushing a button during observation of the ROI in the liver. The elasticity was shown as the speed of the shear wave (m/s) proceeding vertically from the site where ARFI was produced in the liver. Elastography with the ACUSON S2000® was performed at two sites: the right lobe from the intercostal space at a depth of 3 cm from the surface and the left lobe from the median line at a depth of 2 cm from the surface. Liver elasticity was measured 10 times per patient and the median value was recorded. Elasticity was measured simultaneously using the Fibroscan® procedure. Measurement with the Fibroscan® was performed for the right lobe from the intercostal space and the measurement was determined automatically in any 2-cm region in the liver at a depth 2.5–6.5 cm from the surface. The measurement of a patient's liver was performed 10 times and the median value was shown automatically in the window.

We investigated the correlation between the stage of liver fibrosis and the results of elastography measured with the ACUSON S2000® and Fibroscan®. The stage of liver fibrosis was determined according to the METAVIR or New-Inuyama staging by experts in liver pathology [12]. In some samples, the stage of steatohepatitis was also assessed according to Brunt's classification [13]. Biopsy samples less than 1.5 cm in length were excluded.

Blood chemistry and hematologic tests

Blood chemistry and hematologic tests were carried out using conventional autoanalyzers at the same time as the liver stiffness was measured. Data associated with liver stiffness were selected and the results were compared between ARFI and Fibroscan®.

Statistical analysis

Elastography data for each fibrosis stage were calculated and expressed as means ± standard deviation. Correlation between elastography values and fibrosis stage was determined by Kruskal–Wallis analysis and the Jonckheere–Terpstra test. Correlation between the elastography values of ARFI and Fibroscan® was determined by the Pearson product-moment correlation coefficient. A receiver-operating characteristic (ROC) curve was used to determine the best cut-off value for differentiating each F stage and the efficacy was analyzed based on the area under the ROC curve (AUROC) and the likelihood ratio test. The AUROC values of ARFI and Fibroscan® were compared by the χ^2 test. These analyses were performed with SAS computer program software (SAS Institute, Cary, NC, USA).

Results

Patient characteristics

Liver stiffness in the 131 patients with liver damage was measured by ARFI and Fibroscan® at the same time as their percutaneous liver biopsies were performed. The clinical details of these patients are given in Fig. 1. Among the 131 patients, 18 exhibited acute liver damage and were excluded from some of the analyses because it was likely that severe inflammation of the liver would have affected the elastography measurements [14, 15]. Patients with an acute clinical course with the following conditions were included in the analysis : 1 with acute hepatitis A, 1 with acute hepatitis C, 2 with acute hepatitis E, 1 with acute hepatitis due to Epstein-Barr (EB) virus infection, 2 with acute-onset drug-induced liver injury, 2 with acute-onset autoimmune hepatitis, and 9 with acute liver injury of unknown etiology. Among these 18 patients, 2 presented with fulminant liver failure (1 with viral hepatitis and 1 with hepatitis of unknown etiology) and were suspected to have severe fibrosis as a result of severe acute hepatitis. Of the remaining patients, 59 had chronic viral hepatitis (4 were hepatitis B virus-positive and 55 were hepatitis C virus-positive) and 54 were without chronic viral infection (10 had autoimmune hepatitis; 5,primary biliary cirrhosis; 1, primary sclerosing cholangitis; 11, alcoholic liver damage including cirrhosis; 20, non-alcoholic steatohepatitis including cirrhosis; and 7, unknown etiology). The background characteristics of the patients enrolled in the study are shown in Table 1. ARFI measurement was possible in all of these patients; however, Fibroscan® measurement was not possible in 4 patients because of thick subcutaneous fat tissue ($n = 3$) and liver atrophy ($n = 1$).

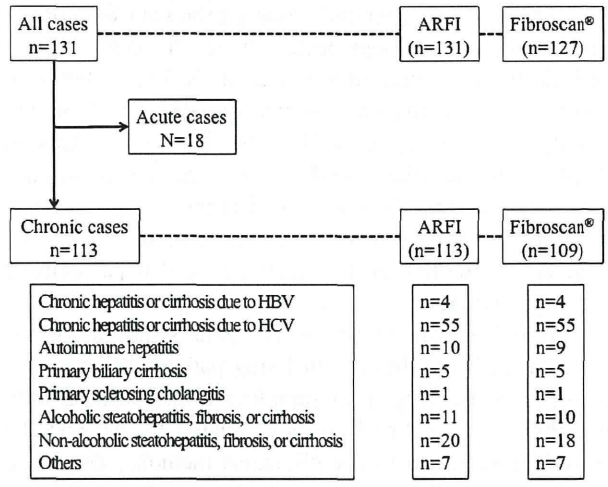

Fig. 1 Characteristics of the patients enrolled in this study. One hundred and thirty-one patients who consented to percutaneous liver biopsy were enrolled. The measurement of liver stiffness by acoustic radiation force impulse (*ARFI*) was possible for all patients, but measurement by Fibroscan® failed for 4 patients because of thick subcutaneous fat tissue ($n = 3$) and liver atrophy ($n = 1$). *HBV* hepatitis B virus, *HCV* hepatitis C virus

Correlation between elastography values and fibrosis stage

Liver stiffness was measured by ARFI with the ACUSON S2000® in the left and right lobes of the liver and by the Fibroscan® method in the right lobe of the liver. ARFI values were determined as velocity (m/s) and Fibroscan® values were determined as elasticity (kPa). Values for the three sets of measurements (ARFI-R (right), ARFI-L (left), and Fibroscan®) increased in proportion to increases in the fibrosis stage (Fig. 2a). The respective mean values for fibrosis stages F0, F1, F2, F3, and F4 were 1.36 ± 0.42, 1.36 ± 0.38, 1.64 ± 0.50, 2.28 ± 0.57, and 2.31 ± 0.78 m/s with ARFI-R ($p < 0.0001$ by Kruskal–Wallis analysis and Jonckheere–Terpstra test), 1.64 ± 0.38, 1.56 ± 0.42, 2.10 ± 0.44, 2.47 ± 0.58, and 2.70 ± 0.68 m/s with ARFI-L ($p < 0.0001$); and 8.4 ± 5.6, 8.4 ± 4.6, 13.1 ± 8.4, 21.1 ± 12.3, and 27.7 ± 16.2 kPa with Fibroscan® ($p < 0.0001$) (Fig. 2a). The Fibroscan® values of patients with acute liver damage were found to be higher than those of patients with chronic liver damage; therefore, we analyzed the data

Table 1 Background characteristics of the patients enrolled in this study

Etiology	Age (years)	Gender (M/F)	Fibrosis (F0/1/2/3/4)	Platelets ($\times 10^3/\mu l$)	Albumin (g/dl)	ALT (IU/l)
Acute ($n = 18$)	57.5 ± 18.0	10/8	9/7/1/1/0	217.1 ± 108.2	3.6 ± 0.6	1059 ± 1290
Chronic ($n = 113$)	64.3 ± 14.3	59/54	10/58/11/16/18	171.7 ± 67.2	4.0 ± 0.5	91 ± 131
CH-B ($n = 4$)	52.3 ± 16.2	4/0	0/2/1/0/1	227.8 ± 91.7	4.2 ± 0.3	296 ± 357
CH-C ($n = 55$)	69.2 ± 12.1	31/24	0/32/6/10/7	148.4 ± 60.2	3.9 ± 0.5	57 ± 41
AIH ($n = 10$)	56.5 ± 13.7	1/9	2/4/1/1/2	173.9 ± 52.3	3.8 ± 0.7	233 ± 290
PBC/PSC ($n = 6$)	54.7 ± 14.6	2/4	1/5/0/0/0	221.5 ± 27.6	4.2 ± 0.1	36 ± 28
ASH/NASH ($n = 31$)	63.7 ± 13.0	16/15	3/13/3/5/7	179.6 ± 61.5	4.2 ± 0.5	84 ± 58
Others ($n = 7$)	54.1 ± 20.5	5/2	4/2/0/0/1	242.3 ± 90.6	3.9 ± 0.3	109 ± 143
Total ($n = 131$)	63.3 ± 14.9	69/62	19/62/13/17/18	177.9 ± 75.3	4.0 ± 0.5	224 ± 587

Acute acute liver injury, *Chronic* chronic liver injury, *CH-B* chronic hepatitis B, *CH-C* chronic hepatitis C, *AIH* autoimmune hepatitis, *PBC* primary biliary cirrhosis, *PSC* primary sclerosing cholangitis, *ASH* alcoholic steatohepatitis, *NASH* non-alcoholic steatohepatitis, *ALT* alanine aminotransferase

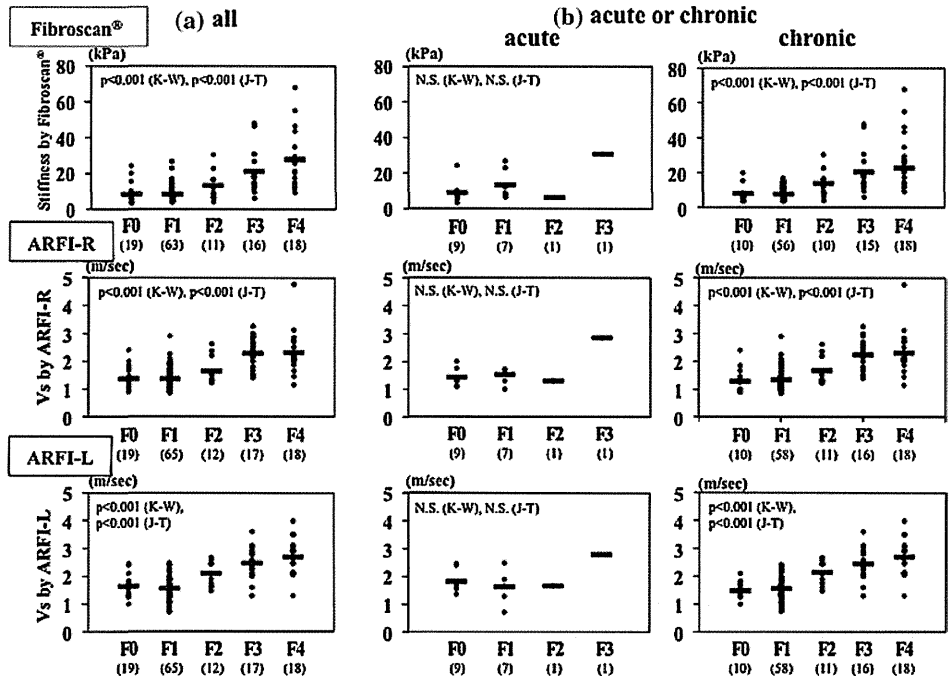

Fig. 2 Correlation between elastography values and fibrosis stage. **a** All patients enrolled in this study, **b** patients stratified by acute and chronic liver injury. The *horizontal lines* indicate the average values of liver stiffness for each stage. Values obtained using the Fibroscan® method increased in proportion to the extent of fibrosis in patients with chronic liver injury ($p < 0.0001$ in chronic liver injury as determined by Kruskal–Wallis (*K-W*) analysis and the Jonckheere–Terpstra (*J-T*) test; not significant (*N.S.*) in patients with acute liver injury). Similar results were seen with acoustic radiation force impulse (right) (*ARFI-R*) ($p < 0.0001$ in chronic liver injury, not significant in acute liver injury) and ARFI (left) (*ARFI-L*) ($p < 0.0001$ in chronic liver injury, not significant in acute liver injury)

separately for patients with acute liver damage and those with chronic liver damage. As reported previously, there was no correlation between the elastography values and the fibrosis stages in patients with acute liver damage (Fig. 2b, left). On the contrary, all these values increased significantly in parallel with the increase in fibrosis stage in patients with chronic liver damage. The respective mean values at fibrosis stages F0, F1, F2, F3, and F4 were 1.29 ± 0.51, 1.35 ± 0.39, 1.68 ± 0.52, 2.24 ± 0.57, and 2.31 ± 0.78 m/s with ARFI-R ($p < 0.0001$); 1.48 ± 0.33, 1.56 ± 0.41, 2.14 ± 0.43, 2.45 ± 0.59, and 2.70 ± 0.68 m/s with ARFI-L ($p < 0.0001$); and 8.0 ± 5.4, 7.7 ± 3.6, 13.9 ± 8.5, 20.5 ± 12.5, and 27.7 ± 16.2 kPa with Fibroscan® ($p < 0.0001$) (Fig. 2b, right).

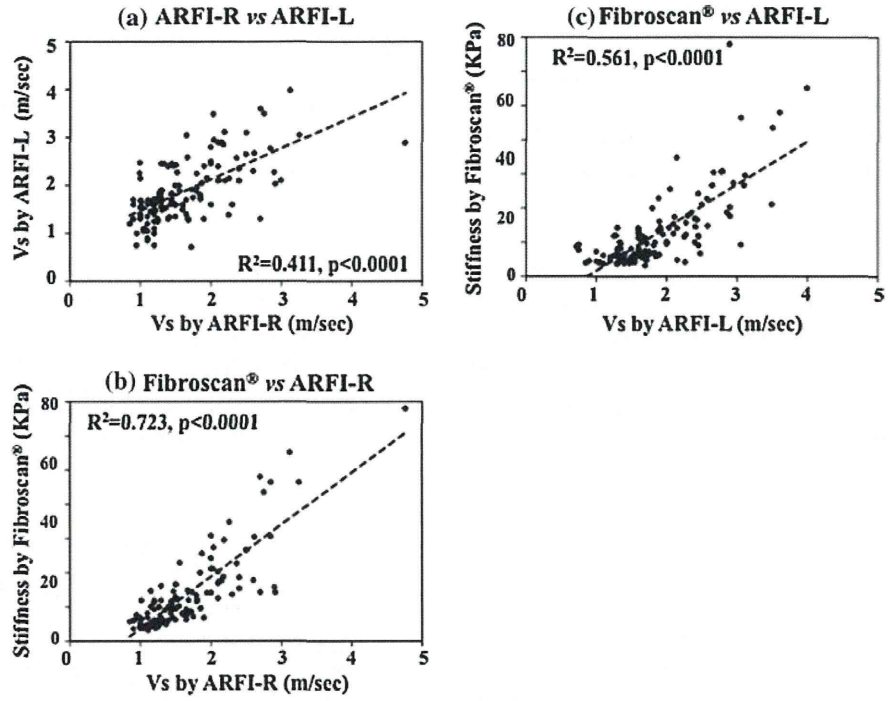

Fig. 3 Correlations between values obtained using the two transient elastography measurement methods. A significant correlation was observed between ARFI-R and ARFI-L values **a** ([ARFI-R] = 0.63[ARFI-L] + 0.45, $R^2 = 0.411$, $p < 0.0001$ by Pearson product-moment correlation coefficient], between ARFI-R and Fibroscan® values **b** ([Fibroscan®] = 15.18[ARFI-R] − 11.54, $R^2 = 0.723$, $p < 0.0001$), and between ARFI-L and Fibroscan® values **c** ([Fibroscan®] = 12.59[ARFI-L] − 10.90, $R^2 = 0.561$, $p < 0.0001$)

We also compared the values of these measurements between patients with acute liver damage and those with chronic liver damage at the same stage of fibrosis (F0 or F1). The values in patients with acute liver damage were greater than those in patients with chronic liver damage, but the only significant difference was for Fibroscan® at stage F1 (data not shown).

Correlation between ARFI and Fibroscan® measurements

Correlations between ARFI-R, ARFI-L, and Fibroscan® values were analyzed. As shown in Fig. 3, significant correlations were evident between ARFI-R and ARFI-L ($R^2 = 0.4109$, $p < 0.0001$ by Pearson product-moment correlation coefficient), ARFI-R and Fibroscan® ($R^2 = 0.7227$, $p < 0.0001$), and ARFI-L and Fibroscan® values ($R^2 = 0.5609$, $p < 0.0001$).

Correlation between values of elastography, blood chemistry, and hematologic test

Because elastography values would be expected to be greater in patients with acute liver damage, the following analyses were performed only for patients with chronic liver damage. In these analyses, ARFI values are represented by ARFI-R values.

We examined the correlation between values of elastography and laboratory tests that are related to liver fibrosis. As shown in Table 2, both Fibroscan® and ARFI-R values were inversely correlated with platelet counts (Fibroscan®: $p < 0.0001$, $R^2 = 0.247$; ARFI-R: $p < 0.0001$, $R^2 = 0.192$ by Pearson product-moment correlation coefficient). In addition, the elastography values were correlated with serum albumin, cholesterol, total bilirubin, γ-globulin level, prothrombin time (international rate), type IV collagen 7S fragment, and hyaluronate (Table 2); the correlations of serological liver fibrosis markers, type IV collagen 7S fragment and hyaluronate, were stronger than those of other

Table 2 Correlation of elastography values with results of blood chemistry and hematology tests (indicated by R^2, * $p < 0.05$ by Pearson product-moment correlation coefficient)

	Fibroscan® ($n = 127$)	ARFI-R ($n = 131$)
Platelet count	0.247*	0.192*
Serum albumin	0.306*	0.232*
AST	0.011	0.019
ALT	0.001	0.003
γ-GTP	0.010	0.031
Total cholesterol	0.130*	0.067*
Total bilirubin	0.235*	0.226*
γ-Globulin	0.086*	0.049*
Prothrombin time	0.173*	0.107*
Type IV collagen 7S	0.575*	0.512*
Hyaluronic acid	0.370*	0.351*

AST aspartate aminotransferase, *γ-GTP* gamma-glutamyl transpeptidase, *ARFI-R* acoustic radiation force impulse (right)

markers tested, and the correlation of Fibroscan® and ARFI-R values were similar.

Overall accuracy of elastography in differentiation between stages of fibrosis

Efficacy was analyzed based on the AUROC, and the best cut-off value for differentiating each F stage was determined (Fig. 4; Table 3a). The accuracy of ARFI-R and Fibroscan® in the diagnosis between F0 and F1–4 was 0.690 and 0.724, respectively. The cut-off values that differentiated between F0 and F1–4 by ROC analysis were 6.2 kPa for Fibroscan® and 1.02 m/s for ARFI-R. For the diagnosis between F0–1 and F2–4 or greater fibrosis stage, the accuracy was 0.891 for Fibroscan® and 0.871 for ARFI-R, and the cut-off values between F0–1 and F2–4 were 9.1 kPa and 1.30 m/s, respectively. In the diagnosis between F0–2 and F3–4 or greater fibrosis stage, accuracy was 0.908 for Fibroscan® and 0.890 for ARFI-R, and the cut-off values between F0–2 and F3–4 were 11.6 kPa and 1.65 m/s, respectively. In the diagnosis of F4 fibrosis stage, accuracy was 0.888 for Fibroscan® and 0.817 for ARFI-R, and the cut-off values between F0–3 and F4 were 14.3 kPa and 1.88 m/s, respectively. The likelihood ratio of a positive test between F0 and F1–4 was low (1.44 for Fibroscan® and 2.25 for ARFI-R), but the likelihood ratio for differentiating between fibrosis stages of F1 and greater were sufficient. Thus, both elastography methods differentiated F1 and greater accurately, but they lacked accuracy in differentiating between F0 and F1.

There were no significant differences in the AUROC values for ARFI-R and Fibroscan® at each fibrosis stage ($p = 0.748$ at F0 and F1–4, $p = 0.512$ at F0–1 and F2–4, $p = 0.344$ at F0–2 and F3–4, $p = 0.908$ at F0–3 and F4, by χ^2 analysis).

Differences in the accuracy of elastography according to the cause of liver damage

This study included patients with liver damage of various causes. Because the pattern of hepatic fibrosis differed between patients with chronic viral hepatitis and those with steatohepatitis (such as alcoholic liver diseases or non-alcoholic steatohepatitis), we examined whether the accuracy of 2 elastography methods was different between patients with chronic viral hepatitis (hepatitis B and C viruses; viral) and those without viral hepatitis (non-viral). Elastography values increased in parallel with the degree of increase in fibrosis in patients with viral hepatitis (viral) and in those without viral hepatitis (non-viral) (Fig. 5). The accuracy of Fibroscan® and ARFI-R for the diagnosis of fibrosis determined by ROC analysis was higher in the patients with viral etiology than in those with non-viral etiology, but both methods were able to distinguish the

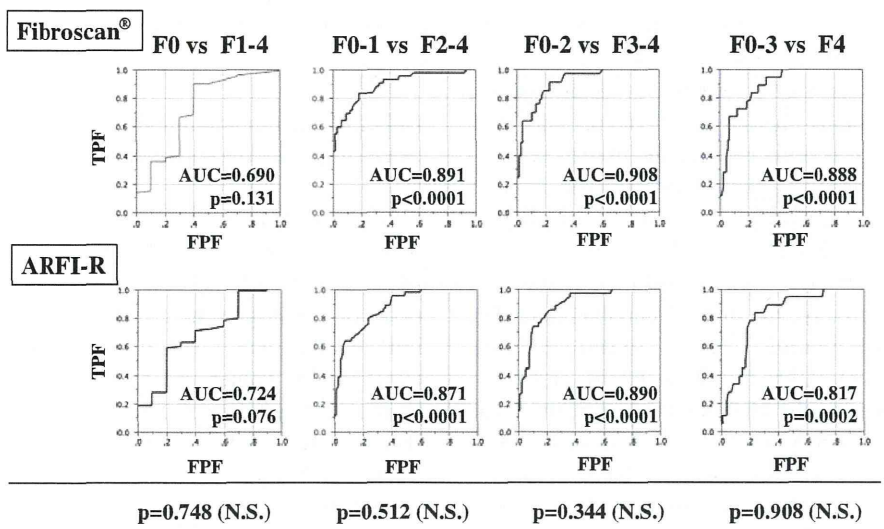

Fig. 4 Accuracy of elastography in differentiating between different stages of fibrosis. The accuracy of differential diagnosis between stage F0 and F1–4 was unsatisfactory with both the Fibroscan® and the ARFI-R methods (area under receiver-operating characteristic curve [AUROC] = 0.690 for Fibroscan®, $p = 0.131$ by χ^2 analysis; AUROC = 0.724 or ARFI-R, $p = 0.076$). However, the accuracy of both methods was sufficient for the diagnosis of stages greater than F2 (Fibroscan®, AUROC = 0.891, $p < 0.0001$; ARFI-R, AUROC = 0.871, $p < 0.0001$), F3 (Fibroscan®, AUROC = 0.908, $p < 0.0001$, ARFI-R, AUROC = 0.890, $p < 0.0001$), or F4 (Fibroscan®, AUROC = 0.888, $p < 0.0001$, ARFI-R, AUROC = 0.817, $p = 0.0002$). There was no significant difference in diagnostic accuracy between the Fibroscan® and ARFI-R methods ($p = 0.748$ for F0 vs. F1–4, $p = 0.512$ for F0–1 vs. F2–4, $p = 0.344$ for F0–2 vs. F3–4, and $p = 0.908$ for F0–3 vs. F4). *AUC* area under curve, *TPF* true positive fraction, *FPF* false positive fraction